JOC The Journal of Organic Chemistry

ACS AUTHORCHOICE

pubs.acs.org/joc Article

How Lewis Acids Catalyze Ring-Openings of Cyclohexene Oxide

Thomas Hansen,[⊥] Pascal Vermeeren,[⊥] Ryoji Yoshisada,[⊥] Dmitri V. Filippov, Gijsbert A. van der Marel, Jeroen D. C. Codée,* and Trevor A. Hamlin*

Cite This: J. Org. Chem. 2021, 86, 3565−3573 Read Online

ACCESS | Metrics & More | Article Recommendations | Supporting Information

ABSTRACT: We have quantum chemically studied the Lewis acid-catalyzed epoxide ring-opening reaction of cyclohexene epoxide by MeZH (Z = O, S, and NH) using relativistic dispersion-corrected density functional theory. We found that the reaction barrier of the Lewis acid-catalyzed epoxide ring-opening reactions decreases upon ascending in group 1 along the series Cs^+ > Rb^+ > K^+ > Na^+ > Li^+ > H^+. Our activation strain and Kohn−Sham molecular orbital analyses reveal that the enhanced reactivity of the Lewis acid-catalyzed ring-opening reaction is caused by the reduced steric (Pauli) repulsion between the filled orbitals of the epoxide and the nucleophile, as the Lewis acid polarizes the filled orbitals of the epoxide more efficiently away from the incoming nucleophile. Furthermore, we established that the regioselectivity of these ring-opening reactions is, aside from the "classical" strain control, also dictated by a hitherto unknown mechanism, namely, the steric (Pauli) repulsion between the nucleophile and the substrate, which could be traced back to the asymmetric orbital density on the epoxide. In all, this work again demonstrates that the concept of Pauli-lowering catalysis is a general phenomenon.

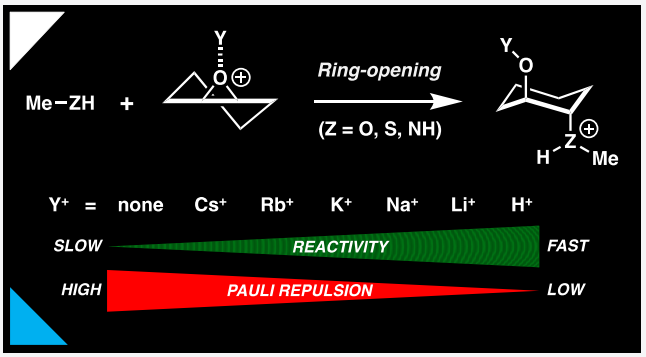

INTRODUCTION

Cyclohexene oxides are valuable building blocks in synthetic chemistry, finding applications in many organic reactions.[1] They can undergo chemical transformations with a broad scope of nucleophiles, making cyclohexene oxides useful building blocks for the synthesis of complex molecules.[2] It is well known that nucleophilic ring-opening reactions of cyclohexene oxides can proceed with excellent regioselectivity.[3] The Fürst-Plattner rule attributes this regiochemical control to a large preference for the reaction pathway that follows the more stable chair-like transition state (*i.e.*, attack at the *α*-position; Scheme 1) compared to the one proceeding through the unfavored twist boat-like transition state (*i.e.*, attack at the *β*-position; Scheme 1).[4] However, despite recent efforts, limited quantitative data is available regarding the origin of the regioselectivity in epoxide ring-opening reactions.[5]

In general, this class of ring-opening reactions is extremely slow and requires a form of activation in order to proceed with efficient conversion.[3] Lewis acids based on group 1 cations (*e.g.*, $LiClO_4$) are popular catalysts to accelerate the reactivity of cyclohexene oxides,[3] and their enhanced reactivity is generally ascribed to the stabilization (*i.e.*, lowering) of the LUMO of the epoxide, which in turn leads to a smaller $HOMO_{nucleophile}$−$LUMO_{epoxide}$ gap and hence a lower ring-opening reaction barrier.[6] In contrast to the current rationale, we have shown recently that Lewis acids do not catalyze organic transformations by enhancing the orbital interactions (*i.e.*, reducing the HOMO−LUMO gap) but instead by diminishing the steric (Pauli) repulsion between the reactants.[7] The complexation between a Lewis acid and the reactant induces a polarization of the occupied orbital densities of the reactant away from the reactive region, resulting in less repulsive occupied−occupied orbital overlap and hence a lower reaction barrier.[7] We envision that this concept of Pauli-repulsion lowering catalysis might also be the driving force in Lewis acid-catalyzed epoxide ring-opening reactions.

To ascertain the universality of this novel Pauli-repulsion lowering catalysis mechanism, we have here performed a comprehensive computational study to unravel the driving force behind Lewis acid-catalyzed cyclohexene oxide ring-opening reactions. In addition, we also studied the physical factors controlling the regioselectivity of this reaction. To this end, we have analyzed the potential energy surfaces of the uncatalyzed and Lewis acid-catalyzed ring-opening reaction of epoxide **1**-Y^+ (Y^+ = none, Cs^+, Rb^+, K^+, Na^+, Li^+, and H^+) by MeZH (Z = O, S, and NH) using relativistic dispersion-corrected density functional theory (Scheme 1). The activation strain model (ASM)[8] of reactivity in combination with Kohn−Sham molecular orbital (KS-MO)[9a] theory and the matching

Received: December 15, 2020
Published: February 4, 2021

https://dx.doi.org/10.1021/acs.joc.0c02955
J. Org. Chem. 2021, 86, 3565−3573

Scheme 1. *α*-Attack (*i.e.*, Chair-Like TS) and *β*-Attack (*i.e.*, Twist Boat-Like TS) of the Lewis Acid-Catalyzed Cyclohexene Oxide Ring-Opening of MeZH with Epoxide-Y^+ (1-Y^+), Where Z = O, S, and NH and Y^+ = none, Cs^+, Rb^+, K^+, Na^+, Li^+, and H^+

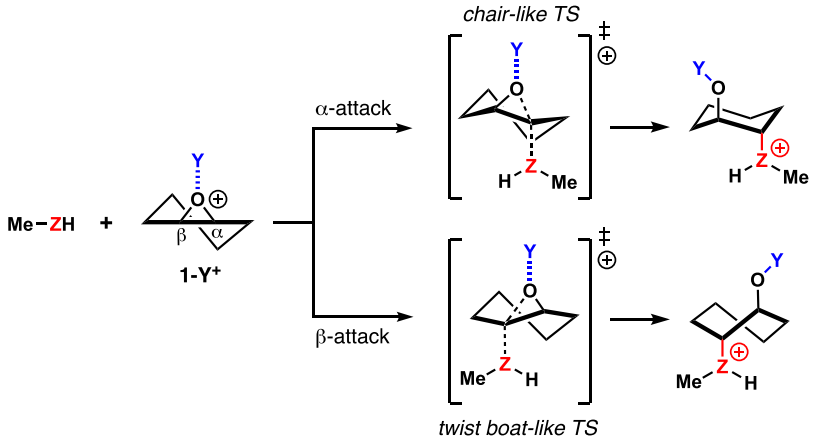

Table 1. Activation Strain Analysis, Energy Decomposition Analysis (in kcal mol^{-1}), and Key Geometrical Details (in Å) for the Interaction between the Lewis Acid Y^+ and Epoxide 1 in the 1-Y^+ Complex[a]

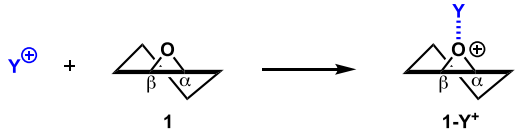

Y^+	ΔE	ΔE_{strain}	ΔE_{int}	ΔV_{elstat}	ΔE_{Pauli}	ΔE_{oi}	r (O···Y^+)	r (C^α–O)[b]	r (C^β–O)[b]
Cs^+	−17.7	0.2	−17.9	−14.9	4.7	−7.7	2.830	1.467	1.461
Rb^+	−19.5	0.2	−19.7	−15.8	4.6	−8.5	2.680	1.468	1.462
K^+	−23.4	0.5	−23.9	−22.0	8.2	−10.1	2.521	1.470	1.464
Na^+	−31.5	0.7	−32.2	−28.3	10.1	−14.0	2.126	1.475	1.469
Li^+	−44.9	1.1	−46.0	−34.8	13.3	−24.5	1.760	1.485	1.479
H^+	−201.3	10.8	−212.1	−40.6	0.0	−171.5	0.983	1.575	1.566

[a]Electronic energies computed at ZORA-M06-2X/TZ2P//B3LYP-D3(BJ)/6-31G+(d), whereas Cs^+ and Rb^+ atoms were treated with the def2-TZVP basis set. [b]In the isolated epoxide **1**, C^α–O = 1.445 Å and C^β–O = 1.438 Å.

energy decomposition analysis (EDA)[9b] scheme were employed to provide quantitative insights into the factors controlling both the catalytic ability and regioselectivity. This computational approach enables the investigation of, and comparison between, activation barriers by decomposing the total energy of the system into physically meaningful terms.[10]

RESULTS AND DISCUSSION

First, we have investigated the strength and nature of the interaction between epoxide (**1**) and the Lewis acid (Y^+), adopting the most stable half-chair conformation of the complex **1**-Y^+ (see Figure S1 for conformational energy landscape (CEL) maps[11]) using a combined activation strain and energy decomposition analysis approach (Table 1).[8,9b] Interestingly, all computed epoxides are asymmetric, that is, the C^α–O bond is longer than the C^β–O bond, which will, as we show later, play a prominent role in the regioselectivity of these epoxide ring-opening reactions. The complexation energies become more stabilizing on ascending in group 1, from −17.7 kcal mol^{-1} for Cs^+ to −201.3 kcal mol^{-1} for H^+, which is exclusively determined by the interaction energy. The strain energy, on the other hand, is marginal and only plays a role when Y^+ = H^+, where a significant $C^{\alpha/\beta}$–O elongation in **1**-H^+ occurs. Notably, the trend in complexation energies (*i.e.*, ΔE) is in line with the trend in alkali metal cation affinities (AMCA) studied by Boughlala *et al.*[12] The O···Y^+ bond length becomes systematically shorter from Cs^+ to H^+, which is in line with the decreasing effective size of the Lewis acid upon ascending in group 1.[12] Both the electrostatic and orbital interactions play an important role in the **1**-Y^+ interaction and become increasingly more stabilizing along Cs^+ to H^+. The stronger electrostatic interaction is a result of a less diffuse electron density and a shorter O···Y^+ bond length. The trend in orbital interactions, which is important for the strength of the catalysis (*vide infra*), can be rationalized by the use of a Kohn–Sham molecular orbital analysis (see Figure S2 in the Supporting Information).[9a,13] The formation of the O···Y^+ bond involves a key donor–acceptor interaction between the oxygen lone pair orbital of **1** (HOMO−1 for Y^+ = Cs^+, Rb^+, K^+, Na^+, and Li^+; HOMO for Y^+ = H^+) and the empty *ns* atomic orbital (AO) of Y^+. The HOMO of the epoxide is a lone pair orbital on the oxygen that is oriented perpendicular to the epoxide ring. The HOMO−1 of the epoxide, on the other hand, is a lone pair orbital on the oxygen oriented in-plane with the epoxide ring (see schematic MOs in Figure S2). H^+ can, due to its lack of electrons and hence no steric (Pauli) repulsion with the C^α and C^β of the epoxide, interact with the higher energy HOMO of the epoxide. The larger group 1 cations, however, do have, if they interact with the HOMO of the epoxide, a significant steric (Pauli) repulsion with the C^α and C^β of the epoxide. To minimize this steric repulsion, the group 1 cation will move away from the C^α and C^β of the epoxide toward the HOMO−1 of the epoxide. Besides reducing the steric repulsion, this displacement of the cation

https://dx.doi.org/10.1021/acs.joc.0c02955
J. Org. Chem. 2021, 86, 3565−3573

Table 2. Energies Relative to Reactants (in kcal mol^{-1}) of the Stationary Points of the Uncatalyzed and Lewis Acid-Catalyzed Epoxide Ring-Opening Reactions between MeZH (Z = O, S, and NH) and 1-Y$^+$ (Y$^+$ = none, Cs$^+$, Rb$^+$, K$^+$, Na$^+$, Li$^+$, and H$^+$)[a]

			Y$^+$					
MeZH	species	none	Cs$^+$	Rb$^+$	K$^+$	Na$^+$	Li$^+$	H$^+$
MeOH	RC	−3.4	−7.0	−7.1	−7.4	−8.0	−8.9	−13.2
	TS-α	53.0	21.5	21.1	19.1	16.1	10.0	−11.7
	TS-β	57.1	28.3	28.1	26.0	19.6	13.1	−8.1
	INT-α	[b]	19.2	18.9	16.4	11.6	1.2	−30.3
	INT-β	57.0	23.8	23.5	21.7	18.6	7.7	−23.8
MeSH	RC	−3.6	−5.6	−5.9	−6.1	−6.5	−7.1	[c]
	TS-α	46.5	20.2	20.1	18.4	15.3	8.9	[c]
	TS-β	50.8	24.9	24.7	22.8	19.7	13.3	[c]
	INT-α	[b]	12.5	12.3	9.7	5.0	−5.6	−38.1
	INT-β	43.6	19.2	19.0	16.3	11.5	0.8	−31.0
$MeNH_2$	RC	−3.4	−6.8	−6.9	−7.2	−7.8	−8.7	[c]
	TS-α	34.4	12.0	11.7	10.0	6.6	0.5	[c]
	TS-β	38.5	16.0	15.6	13.9	10.6	4.4	[c]
	INT-α	24.6	−10.7	−10.9	−13.7	−18.5	−29.4	−62.2
	INT-β	31.1	−4.2	−4.4	−7.1	−12.0	−22.9	−55.0

[a]Electronic energies computed at M06-2X/6-311++G(d,p)//B3LYP-D3(BJ)/6-31G+(d), whereas Cs$^+$ and Rb$^+$ atoms were treated with the def2-TZVP basis set (see Figure 1 for designation of species). [b]Nonexistent: formation of the zwitterionic INT-α is unstable, which decomposes barrierless in a cyclohexanone-like species and H_2. [c]Nonexistent: barrierless process toward an INT.

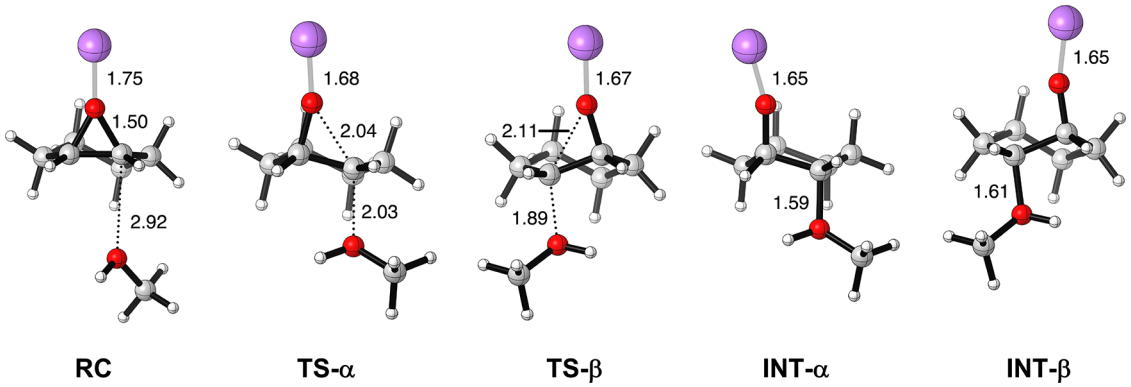

Figure 1. Structures and key distances (in Å) of stationary points of the Lewis acid-catalyzed epoxide ring-opening reactions between MeOH and **1-Li**$^+$ computed at B3LYP-D3(BJ)/6-31G+(d).

also results in a loss of a favorable orbital overlap between the empty *ns* atomic orbital (AO) of the group 1 cation and the HOMO of the epoxide, but it will gain a stabilizing orbital overlap between the *ns* AO of the group 1 cation and the HOMO−1 of the epoxide (see Figure S2). The key orbital overlap increases from 0.06 for Cs$^+$ to 0.33 for H$^+$ due to the more compact nature of the empty *ns* AO of **Y**$^+$ when ascending in group 1.[12] In addition, the orbital energy gap also becomes smaller, going from Cs$^+$ to H$^+$, because of the consistently more stable empty *ns* AO of **Y**$^+$, which further contributes to a more stabilizing orbital interaction in the case of lighter Lewis acids.

Table 2 and Figure 1 summarize the computed reaction profiles and structural data of the Lewis acid-catalyzed epoxide ring-opening reactions between MeZH (Z = O, S, and NH) and **1-Y**$^+$, forming the α- and β-intermediate. Three distinct trends can be observed. In the first place, the nucleophilic attack can occur at both the α- and β-carbon of the epoxide ring, of which, for all computed systems, the α-attack occurs with a 3−7 kcal mol^{-1} lower reaction barrier than the β-attack. Second, the reaction barrier systematically decreases when **Y**$^+$ ascends group 1 (Cs$^+$ > Rb$^+$ > K$^+$ > Na$^+$ > Li$^+$ > H$^+$). This is in good agreement with the experimentally determined reactivity trends for Lewis acid-catalyzed epoxide ring-opening reactions, which showed that the H$^+$-catalyzed epoxide ring-opening reaction can already be performed at room temperature within 30 min, while the Li$^+$- and Na$^+$-catalyzed analogs require an elevated temperature and a significantly longer reaction time. The reactions catalyzed by K$^+$, Rb$^+$, and Cs$^+$, on the other hand, are experimentally not used due to their poor catalytic ability.[3] For the more nucleophilic MeSH and $MeNH_2$, the reaction barrier decreases along the series of **Y**$^+$ to such an extent that the epoxide ring-opening reaction catalyzed by H$^+$ is barrierless. Third, when changing the nucleophile from MeOH to MeSH and to $MeNH_2$, the reaction barriers of all epoxide ring-opening reactions become lower due to the enhanced nucleophilicity whereby the nucleophile can engage in a stronger acid−base-like interaction with the substrate **1-Y**$^+$.[10b] In our following detailed analysis, we will solely focus on the epoxide ring-opening reactions by MeOH;[3] however, note that the other nucleophiles (*i.e.*, MeSH and $MeNH_2$) possess the same reactivity and regioselectivity trends (for the detailed analysis of MeSH and $MeNH_2$, see Table S1 in the Supporting Information).

https://dx.doi.org/10.1021/acs.joc.0c02955
J. Org. Chem. 2021, 86, 3565−3573

Next, we turn to the activation strain model (ASM)[8] of reactivity to gain quantitative insights into the physical factors controlling the regiochemical preference for the epoxide ring-opening at the α-position. In Figure 2a, we focus on the Li^+-catalyzed epoxide ring-opening reaction. Note that the ASM results of the uncatalyzed and the other Lewis acid-catalyzed epoxide ring-opening reactions possess the same characteristics and are shown in Table S2 in the Supporting Information. In line with Table 2, we observe that the α-attack (black) goes with a lower reaction barrier than the β-attack (red) since the black dot, which indicates the transition state, is below the red analog. This trend in regiochemical preference is originating from both a less destabilizing activation strain and a more stabilizing interaction energy because the black interaction and strain energy curves, corresponding to the α-attack, are below the red counterparts. The less destabilizing strain energy for the α-attack can be rationalized by means of the Fürst-Plattner rule, which postulates that the α-attack goes via a more stable chair-like transition state and is, therefore, accompanied with less activation strain, whereas the β-attack follows a more distorted (*i.e.*, destabilized) twist boat-like transition state.[4] This is corroborated by the fact that the C^{α}–O bond is significantly weaker compared to the C^{β}–O bond (C^{α}–O: ΔH_{BDE} = 60.3 kcal mol^{-1} and C^{β}–O: ΔH_{BDE} = 63.3 kcal mol^{-1}). This effect can also already be found in the reactants (*i.e.*, **1-Y**$^+$), the epoxide releases some of the unfavorable ring strain of the three-membered ring, predistorting toward the more stable chair-like structure, which is effectively asymmetric, that is, the C^{α}–O bond is longer than the C^{β}–O bond.

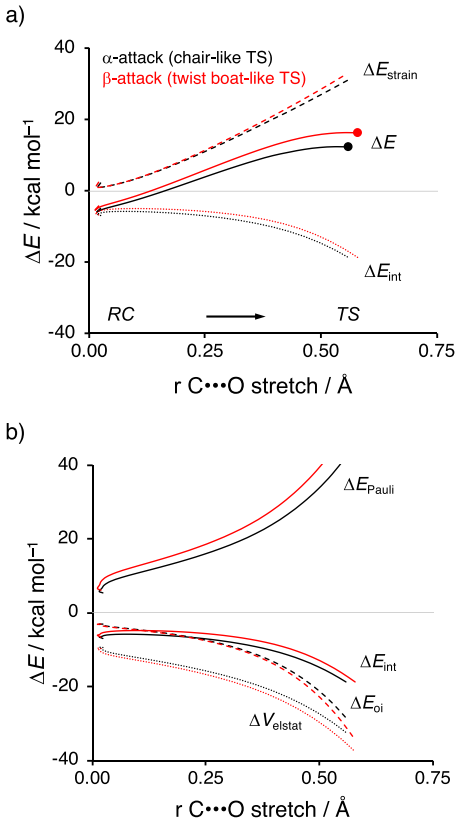

Figure 2. (a) Activation strain model, where ΔE = solid lines, ΔE_{strain} = dashed lines, and ΔE_{int} = dotted lines. (b) Energy decomposition analysis, where ΔV_{elstat} = dotted lines, ΔE_{Pauli} = solid lines, and ΔE_{oi} = dashed lines, for the Lewis acid-catalyzed ring-opening reactions of MeOH and **1-Li**$^+$ via the α-attack (black; chair-like TS) and β-attack (red; twist boat-like TS), where the energy values are plotted from the reactant complex to the transition state (indicated by a dot) and projected onto the $C^{\alpha/\beta}$···O bond stretch. The transition states are indicated by a dot. Computed at ZORA-M06-2X/TZ2P//B3LYP-D3(BJ)/6-31G+(d).

To understand why the α-attack benefits from a more stabilizing interaction energy than the β-attack, a hitherto unknown factor that participates in determining the regioselectivity, we employed our energy decomposition analysis (EDA).[9b] Interestingly, we found that the α-attack (black) goes with significantly less destabilizing Pauli repulsion compared to the β-attack (red) since the black Pauli repulsion curve is, along the entire reaction coordinate, lower in energy (*i.e.*, less destabilizing) than the red curve (Figure 2b). In other words, for the attack at the α-position, the nucleophile and **1-Li**$^+$ experience less steric repulsion than for the attack at the β-position. The attractive electrostatic and orbital interactions are, on the other hand, slightly more stabilizing for the β-attack, showing a trend opposite of the trend in interaction energy, and hence not responsible for the observed regioselectivity.

The origin of the less destabilizing Pauli repulsion for the attack at the α-position compared to the β-position was further investigated by performing a Kohn–Sham molecular orbital analysis.[9a,13] The occupied orbitals of MeOH and **1-Li**$^+$, for both the attack at the α- and β-position, were quantified at transition state-like, consistent geometries with a $C^{\alpha/\beta}$···O bond stretch of 0.54 Å (Figure 3). The most important occupied molecular orbitals (MOs) that dictate the trend in Pauli repulsion, that is, the occupied orbitals responsible for the differences in steric repulsion between the reactant along the different regiochemical reaction pathways, are the HOMO−7 of **1-Li**$^+$ and the HOMO and HOMO−6 of MeOH. The $HOMO_{MeOH}$ is an oxygen lone pair orbital and the $HOMO-6_{MeOH}$ is an all in-phase σ-orbital, whereas the $HOMO-7_{1\text{-}Li+}$ is a filled σ-orbital delocalized over the cyclohexane ring of **1-Li**$^+$ (Figure 3b). As shown in Figure 3a, the occupied–occupied orbital overlap between these orbitals is nonexistent for the α-attack (S = 0.00 and S = 0.00), while it is present, and hence destabilizing, for the β-attack (S = 0.03 and S = 0.02). The asymmetry in the $C^{\alpha/\beta}$–O bond lengths of **1-Li**$^+$ induces an asymmetry in the $HOMO-7_{1\text{-}Li+}$, namely, there is more orbital density located on the carbon atom participating in the shorter epoxide C^{β}–O bond (β-carbon) than on the carbon atom involved in the longer epoxide C^{α}–O bond (α-carbon). Thus, when MeOH attacks the β-position, it encounters and hence overlaps with the large occupied orbital amplitude of the $HOMO-7_{1\text{-}Li+}$ located on the β-carbon, manifesting in more destabilizing Pauli repulsion and a higher reaction barrier compared to the α-attack.

After having established that the nucleophile preferentially opens the epoxide at the α-position, we analyze the reactivity trends of this reaction pathway for all six Lewis acids (Y^+ = Cs^+, Rb^+, K^+, Na^+, Li^+, and H^+) and for the uncatalyzed reaction (Y^+ = none). Figure 4a shows the activation strain model (ASM) results from the reactant complexes to the transition states for the uncatalyzed and Cs^+- and H^+-catalyzed epoxide ring-opening reactions (see Table S3 and Figure S4 in the Supporting Information for all ASM results). The uncatalyzed reaction (black) goes with the highest reaction barrier, and coordinating a Cs^+ cation (orange) lowers the barrier, which then consistently decreases upon ascending in

https://dx.doi.org/10.1021/acs.joc.0c02955
J. Org. Chem. 2021, 86, 3565−3573

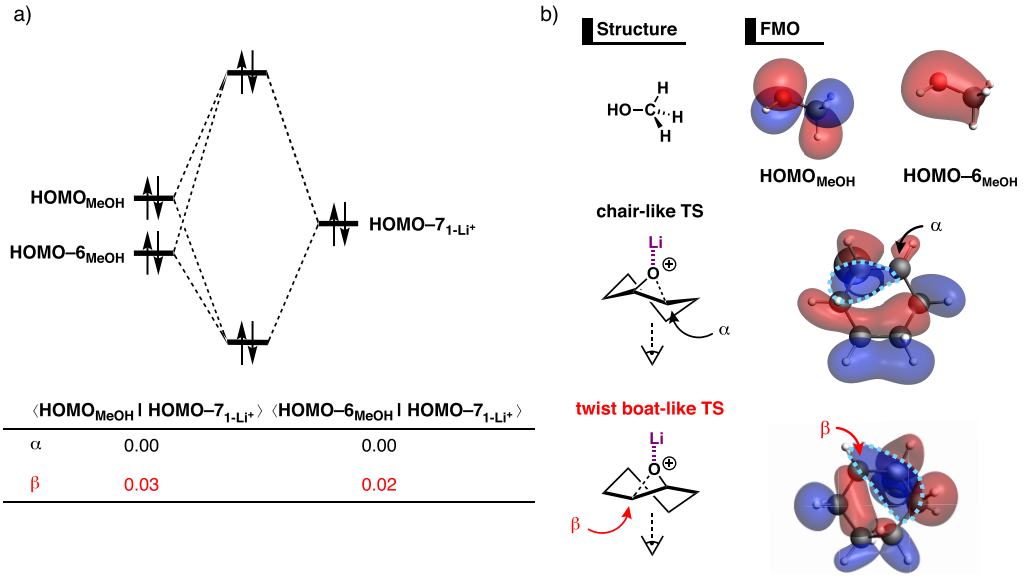

Figure 3. (a) Molecular orbital diagram of the most important occupied−occupied orbital overlap for the Lewis acid-catalyzed ring-opening reactions of the α- and β-attack for MeOH +**1**-Li$^+$. (b) Key occupied orbital (isovalue = 0.03 Bohr$^{-3/2}$) computed at consistent TS-like geometries with a C$^{\alpha/\beta}$···O bond stretch of 0.54 Å, in which **1**-Li$^+$ is depicted from the bottom side. Computed at ZORA-M06-2X/TZ2P//B3LYP-D3(BJ)/6-31G+(d).

group 1. The lowest reaction barrier, however, can be found for the H$^+$-catalyzed (red) epoxide ring-opening reaction. The enhanced reactivity (*i.e.*, the catalysis) originates from both a less destabilizing strain energy and more stabilizing interaction energy along the entire reaction coordinate because the orange and red strain and interaction energy curves, corresponding to the LA-catalyzed epoxide ring-opening reactions, are below the black counterparts. The less destabilizing strain energy for the reaction catalyzed by a Lewis acid is directly related to the donor−acceptor interaction in the complexation between **Y**$^+$ and **1** (Table 1), which is able to stabilize the evolving negative charge localizing on the oxygen atom of the epoxide upon ring-opening. Thus, in other words, the coordinating Lewis acid makes the epoxide oxygen a "better leaving group" and, therefore, lowers the activation strain of the ring-opening reaction.[10d] This effect becomes more pronounced when the donor−acceptor interaction increases between **Y**$^+$ and **1**.

Our EDA reveals that the more stabilizing interaction energy of the Lewis acid-catalyzed ring-opening reactions originates predominantly from a less destabilizing Pauli repulsion since the orange and red Pauli repulsion curves are, along the entire reaction coordinate, significantly lower in energy (*i.e.*, less destabilizing) than the black curve (Figure 4b). The orbital interactions, which are commonly seen as the driving force behind this catalysis, only have a minor contribution to the trend in interaction energy. Note, however, that these EDA results should be carefully interpreted. In our recent work on epoxide ring-opening reactions under basic and acidic conditions, we showed that the results of the EDA are also highly influenced by the nucleophile−substrate distance,[10a] which is in this work almost 0.1 Å longer for **1** compared to **1**-H$^+$ (1.98 Å for **1** and 2.05 Å for **1**-H$^+$) at a C$^\alpha$···O bond stretch of 0.59 Å. To assess the potential influence of different MeOH···**1**-Y$^+$ distances on the EDA results, we performed a numerical experiment where we artificially constrained the MeOH···C$^\alpha$ bond length of all reactions to the MeOH···C$^\alpha$ bond length of **1** (1.98 Å) while keeping the C$^\alpha$···O bond stretch consistent at 0.59 Å (Table S3 in the Supporting Information). A constrained MeOH···C$^\alpha$ bond length of 1.98 Å was judiciously selected because it provided transition-like geometries that are the closest to the transition states of all systems studied in this work. The corresponding EDA results are fully consistent with the EDA diagram of Figure 4, indicating that the trend in interaction energy is, indeed, predominantly originating from the lowering of the Pauli repulsion. The orbital interactions, on the other hand, also become slightly more stabilizing from **Y**$^+$ = none to **Y**$^+$ = H$^+$ due to the ability of the Lewis acid to induce a lowering of the LUMO$_{1\text{-}Y+}$ as is the common explanation in the literature.[6] More importantly, the stabilization originating from the stronger orbital interactions is, however, an order of magnitude smaller than the stabilization due to the reduction of Pauli repulsion and is, therefore, not the main actor behind the rate enhancement of the Lewis acid-catalyzed epoxide ring-opening reactions.

The reduction in destabilizing Pauli repulsion upon going from the uncatalyzed to the Lewis acid-catalyzed ring-opening reactions, and hence the origin of the catalysis along the series, derives from a reduced occupied−occupied orbital overlap (*i.e.*, steric interaction) between **1**-**Y**$^+$ and the incoming MeOH. The two-center four-electron repulsive interaction between the occupied orbitals of MeOH and **1**-**Y**$^+$ was quantified at double consistent geometries with a C$^\alpha$···O bond stretch of 0.59 Å and MeOH···C$^\alpha$ bond length of 1.98 Å to eliminate any potential influence of different MeOH···**1**-**Y**$^+$ distances (Figure 5; *vide supra*). The FMO$_{1\text{-}Y+}$ (*i.e.*, HOMO or HOMO−1) has two occupied−occupied orbital overlaps that are decisive for the trend in Pauli repulsion, namely, with the HOMO$_{MeOH}$ and HOMO−6$_{MeOH}$. The respective orbital overlap and hence repulsion are the largest and most destabilizing for the uncatalyzed reaction (S = 0.07 and 0.09) and the smallest and least destabilizing for the H$^+$-catalyzed reaction (S = 0.01 and 0.02) (Figure 5a). In line with our previous work,[7] we found that by coordinating a Lewis acid to **1**, the σ-orbital of **1** becomes polarized away from the incoming MeOH due to both the positive potential of the cationic Lewis acid and the

https://dx.doi.org/10.1021/acs.joc.0c02955
J. Org. Chem. 2021, 86, 3565−3573

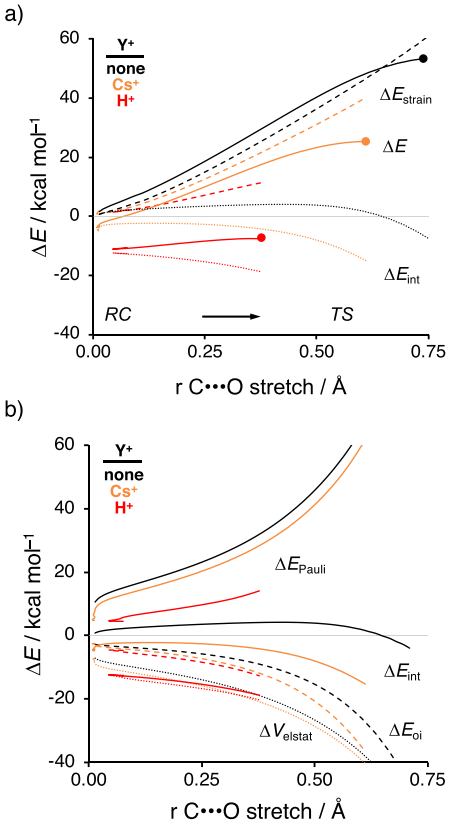

Figure 4. (a) Activation strain model, where ΔE = solid lines, ΔE_{strain} = dashed lines, and ΔE_{int} = dotted lines. (b) Energy decomposition analysis, where ΔV_{elstat} = dotted lines, ΔE_{Pauli} = solid lines, and ΔE_{oi} = dashed lines, for the uncatalyzed and Lewis acid-catalyzed ring-opening reactions of MeOH +**1**-$\mathbf{Y}^+$ via the α-attack ($\mathbf{Y}^+$ = none, black; Cs^+, orange; and H^+, red), where the energy values are plotted from the reactant complex to the transition state and projected onto the C^α···O bond stretch. The transition states are indicated by a dot. Computed at ZORA-M06-2X/TZ2P//B3LYP-D3(BJ)/6-31G+(d), whereas the Cs^+ atom is treated with the def2-TZVP basis set.

donor–acceptor interaction between the empty *ns* AO of the Lewis acid and the filled orbitals of **1**. The effect of the positive potential on the σ-orbital of **1** is strongly related to the distance between the Lewis acid and **1**. Thus, the shorter the O···$\mathbf{Y}^+$ bond length when going to lighter cations, the greater the extent of σ-orbital polarization induced by the positive potential (see Figure S5 in the Supporting Information). Furthermore, the strength of the donor–acceptor interaction, as discussed during the analysis of the **1**-$\mathbf{Y}^+$ complexation, systematically increases upon ascending in group 1, from −7.7 kcal mol^{-1} for Cs^+ to −171.5 kcal mol^{-1} for H^+ (see Table 1). These two mechanisms result in a consistently smaller $FMO_{\mathbf{1}\text{-}\mathbf{Y}+}$ orbital amplitude pointing toward the attacking MeOH. This can be seen when comparing the size of the red lobes with a blue dashed outline on the C^α–C^β bond of the corresponding **1**-$\mathbf{Y}^+$ orbital densities (Figure 5b). These results clearly illustrate that the concept of Pauli-lowering catalysis is a general phenomenon that is not only limited to Lewis acid-catalyzed Michael addition and cycloaddition reactions.[7]

CONCLUSIONS

Our computational study reveals that Lewis acids ($\mathbf{Y}^+$) efficiently catalyze the nucleophilic ring-opening reactions of cyclohexene oxides. The reaction barrier of the Lewis acid-catalyzed epoxide ring-opening reaction decreases upon ascending in group 1 along the series $Cs^+ > Rb^+ > K^+ > Na^+ > Li^+ > H^+$. Furthermore, we found that the reaction pathway following a chair-like transition state goes, for all studied systems, with a significantly lower reaction barrier than the twist boat-like analog.

Our activation strain and Kohn–Sham molecular orbital analyses showed that, in contrast to the generally accepted belief, the catalytic ability of the Lewis acids is caused by the reduction of steric (Pauli) repulsion between the Lewis acid-activated epoxide **1**-$\mathbf{Y}^+$ and the nucleophile and not by the enhanced stabilizing orbital interactions as is currently the prevailing mechanism in the literature. The reduction in steric (Pauli) repulsion can be traced back to the Lewis acid-induced polarization of the occupied orbitals on **1**-$\mathbf{Y}^+$ away from the incoming nucleophile. This effect gets more pronounced ascending in group 1 because the positive potential of the lighter cations polarizes due to the shorter O···$\mathbf{Y}^+$ bond, the occupied orbitals on **1**-$\mathbf{Y}^+$ to a greater extent and their lower-energy valence *ns* AOs engage in a stronger donor–acceptor interaction with the occupied orbitals of epoxide **1**-$\mathbf{Y}^+$. This again demonstrates that Pauli-lowering catalysis is a general phenomenon, which is not only limited to Michael addition reactions and cycloadditions.

In addition, we discovered a novel physical mechanism that is responsible for the regioselectivity of the cyclohexene oxides ring-opening that acts aside from the Fürst-Plattner rule, which proposes that the regioselectivity is solely determined by the strain of the associated reaction paths. Instead, we found that regioselectivity for nucleophilic attack at the C^α and C^β of the epoxide **1**-$\mathbf{Y}^+$ is, to a substantial degree, controlled by the steric (Pauli) repulsion between **1**-$\mathbf{Y}^+$ and the nucleophile. This effect originates from the asymmetry of the epoxide $C^{\alpha/\beta}$–O bonds in **1**-$\mathbf{Y}^+$, which results in more orbital amplitude on the β-carbon and hence a significant steric interaction with the incoming nucleophile attacking the β-carbon. These findings will equip experimentalists with the mechanistic insight to understand and rationalize the trends in reactivity as well as regioselectivity of both uncatalyzed and Lewis acid-catalyzed epoxide ring-opening reactions.

METHODS

Computational Details. Computations were performed using Gaussian 09 Rev. D.01.[14] using the hybrid functional B3LYP-D3(BJ)[15] with 6-31+G(d)[16] as a basis set for geometry optimization. More accurate electronic energies were obtained by a single-point calculation with M06-2X[17] with 6-311++G(d,p)[16] for all atoms, except for Cs^+ and Rb^+, which were treated with def2-TZVP.[18] This approach proved to give an excellent trade-off between accuracy and computational time.[19] The geometry convergence criteria were set to tight (max. force = $1.5{\cdot}10^{-7}$, max. displacement = $6.0{\cdot}10^{-7}$), and an internally defined superfine grid size was used (Int = veryfinegrid), which is a pruned 175,974 grid for first-row atoms and a 250,974 grid for all other atoms. These parameters were chosen as a recent paper indicated a significant dependence of the computed frequencies on the molecule orientation when a smaller grid size is used.[20] Geometries were optimized without symmetry constraints. The quasi-harmonic correction[21] was applied to all frequencies by modifying all vibration below 100 cm^{-1} to 100 cm^{-1}. All computed stationary points have been confirmed by performing a vibrational analysis calculation. The energy minima had no imaginary frequencies, while the transition states had only one imaginary frequency. The character of the normal mode associated with the transition state's imaginary frequency has been inspected to ensure that it corresponds to the reaction of interest. The potential energy

https://dx.doi.org/10.1021/acs.joc.0c02955
J. Org. Chem. 2021, 86, 3565–3573

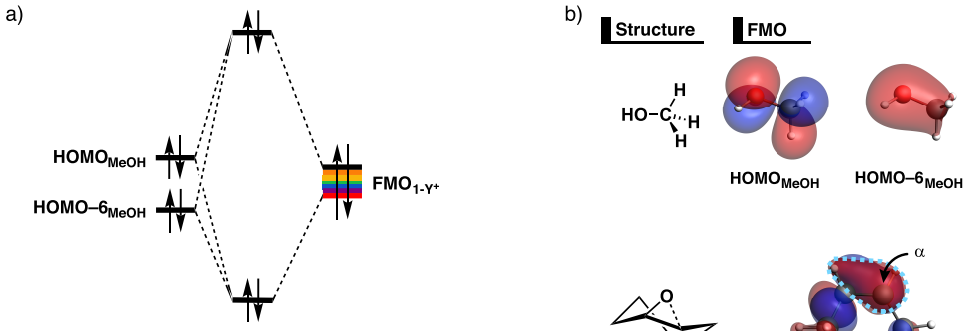

Y$^+$	FMO$_{1\text{-}Y^+}$	⟨HOMO$_{MeOH}$ I FMO$_{1\text{-}Y^+}$⟩	⟨HOMO–6$_{MeOH}$ I FMO$_{1\text{-}Y^+}$⟩
none	HOMO–1	0.07	0.09
Cs$^+$	HOMO–1	0.06	0.07
Rb$^+$	HOMO–1	0.05	0.07
K$^+$	HOMO–1	0.05	0.07
Na$^+$	HOMO–1	0.04	0.06
Li$^+$	HOMO–1	0.03	0.05
H$^+$	HOMO	0.01	0.02

Figure 5. (a) Molecular orbital diagram of the most important occupied−occupied orbital overlap for the uncatalyzed and Lewis acid-catalyzed ring-opening reactions of MeOH +**1**-Y$^+$ (Y$^+$ = none, Cs$^+$, Rb$^+$, K$^+$, Na$^+$, Li$^+$, and H$^+$). (b) Key occupied orbital (isovalue = 0.03 Bohr$^{-3/2}$) computed at consistent TS-like geometries with a C$^\alpha$···O stretch of 0.59 Å and MeOH···C$^\alpha$ bond length of 1.98 Å. The key filled orbital lobe of **1**-Y$^+$, which has an overlap with the filled orbitals of the incoming MeOH, is highlighted with a blue dashed outline. Computed at ZORA-M06-2X/TZ2P//B3LYP-D3(BJ)/6-31G+(d), whereas Cs$^+$ and Rb$^+$ atoms were treated with the def2-TZVP basis set.

surfaces of the studied epoxide ring-opening reactions were obtained by performing intrinsic reaction coordinate (IRC) calculations. The activation strain analysis (ASM)[8] of reactivity and energy decomposition analysis (EDA)[9] were performed using the Amsterdam Density Functional (ADF2017.103) software package[22] together with the PyFrag 2019.[23] These analyses were utilized using the M06-2X functional together with the triple-ζ quality TZ2P basis set[24] on the geometries optimized at B3LYP-D3(BJ)/6-31G+(d). The zeroth-order regular approximation (ZORA) was applied to account for scalar relativistic effects.[25] The accuracies of the fit scheme and the integration grid, the Zlm fit and Becke grid, were set to VERYGOOD.[26] The optimized structures were illustrated using CYLview.[27]

Activation Strain and Energy Decomposition Analysis. The activation strain model (ASM)[8] of reactivity, also known as the distortion/interaction model,[28] is a fragment-based approach based on the idea that the energy of an interaction system, *i.e.*, the potential energy surface, can be described and understood by looking at the original reactants. It considers the rigidity and their capability to interact as the reaction proceeds along the reaction coordinate. In this model, the total energy, $\Delta E(\zeta)$, is being decomposed into the strain and interaction energy, $\Delta E_{strain}(\zeta)$ and $\Delta E_{int}(\zeta)$, respectively, and these values are projected onto the reaction coordinate ζ [eq 1]:

$$\Delta E(\zeta) = \Delta E_{strain}(\zeta) + \Delta E_{int}(\zeta) \quad (1)$$

Herein, the strain energy, $\Delta E_{strain}(\zeta)$, is the penalty that needs to be paid in order to deform the reactants from their equilibrium structure to their respective geometry that they adopt during the reaction at point ζ of the reaction coordinate. On the other hand, the interaction energy, $\Delta E_{int}(\zeta)$, accounts for all the mutual interactions that occur between these deformed reactants along the reaction coordinate.

The interaction energy between the deformed reactants can be further analyzed in terms of quantitative Kohn−Sham molecular orbital theory (KS-MO) in combination with a canonical energy decomposition analysis (EDA).[9] The EDA decomposes the $\Delta E_{int}(\zeta)$ into three physically meaningful energy terms [eq 2]:

$$\Delta E_{int}(\zeta) = \Delta V_{elstat}(\zeta) + \Delta E_{Pauli}(\zeta) + \Delta E_{oi}(\zeta) \quad (2)$$

In eq 2, $\Delta V_{elstat}(\zeta)$ is the classical electrostatic interaction between the unperturbed charge distributions of the (deformed) reactants and is usually attractive. The Pauli repulsion, $\Delta E_{Pauli}(\zeta)$, describes the destabilizing interaction between fully occupied closed-shell orbitals of both fragments due to Pauli's principle. The orbital interaction energy, $\Delta E_{oi}(\zeta)$, accounts for polarization and charge transfer between the fragments, such as HOMO−LUMO interactions.

In the activation strain and accompanied energy decomposition diagrams presented in this work, the various energy terms are projected onto the carbon−oxygen (C$^{\alpha/\beta}$−O) distance. This critical reaction coordinate undergoes a well-defined change during the reaction from the reactant complex via the transition state to the product and is shown to be a valid reaction coordinate for studying nucleophilic substitution reactions.[10]

Thermochemistry. Bond enthalpies, *i.e.*, bond dissociation energies (BDE), are calculated at 298.15 K and 1 atm (ΔH_{BDE}) from electronic bond energies (ΔE) and vibrational frequencies using standard thermochemistry relations for an ideal gas [eq 3][29]

$$\Delta H_{BDE} = \Delta E + \Delta E_{trans,298} + \Delta E_{rot,298} + \Delta E_{vib,0} + \Delta(\Delta E_{vib,0})_{298} \quad (3)$$

Here, $\Delta E_{trans,298}$, $\Delta E_{rot,298}$, and $\Delta E_{vib,0}$ are the differences between the epoxide and the ring-opened diradical that results from breaking either the C$^\alpha$−O or C$^\beta$−O bond in translational, rotational, and zero-point vibrational energy, respectively. The last term, $\Delta(\Delta E_{vib,0})_{298}$, is the change in the vibrational energy difference when going from 0 K to 298.15 K.

■ ASSOCIATED CONTENT

Supporting Information

The Supporting Information is available free of charge at https://pubs.acs.org/doi/10.1021/acs.joc.0c02955.

Additional computational results and Cartesian coordinates, energies, and number of imaginary frequencies of all stationary points (PDF)

https://dx.doi.org/10.1021/acs.joc.0c02955
J. Org. Chem. 2021, 86, 3565−3573

AUTHOR INFORMATION

Corresponding Authors

Jeroen D. C. Codée − *Leiden Institute of Chemistry, Leiden University, 2333 CC Leiden, The Netherlands;* orcid.org/0000-0003-3531-2138; Email: jcodee@chem.leidenuniv.nl

Trevor A. Hamlin − *Department of Theoretical Chemistry, Amsterdam Institute of Molecular and Life Sciences (AIMSS), Amsterdam Center for Multiscale Modeling (ACMM), Vrije Universiteit Amsterdam, 1081 HV Amsterdam, The Netherlands;* orcid.org/0000-0002-5128-1004; Email: t.a.hamlin@vu.nl

Authors

Thomas Hansen − *Department of Theoretical Chemistry, Amsterdam Institute of Molecular and Life Sciences (AIMSS), Amsterdam Center for Multiscale Modeling (ACMM), Vrije Universiteit Amsterdam, 1081 HV Amsterdam, The Netherlands; Leiden Institute of Chemistry, Leiden University, 2333 CC Leiden, The Netherlands;* orcid.org/0000-0002-6291-1569

Pascal Vermeeren − *Department of Theoretical Chemistry, Amsterdam Institute of Molecular and Life Sciences (AIMSS), Amsterdam Center for Multiscale Modeling (ACMM), Vrije Universiteit Amsterdam, 1081 HV Amsterdam, The Netherlands;* orcid.org/0000-0002-2100-6837

Ryoji Yoshisada − *Leiden Institute of Chemistry, Leiden University, 2333 CC Leiden, The Netherlands*

Dmitri V. Filippov − *Leiden Institute of Chemistry, Leiden University, 2333 CC Leiden, The Netherlands;* orcid.org/0000-0002-6978-7425

Gijsbert A. van der Marel − *Leiden Institute of Chemistry, Leiden University, 2333 CC Leiden, The Netherlands*

Complete contact information is available at: https://pubs.acs.org/10.1021/acs.joc.0c02955

Author Contributions

⊥T.H., P.V., and R.Y. contributed equally to this work.

Notes

The authors declare no competing financial interest.

ACKNOWLEDGMENTS

We thank the Netherlands Organization for Scientific Research (NWO) and the Dutch Astrochemistry Network (DAN) for financial support. Quantum chemical calculations were performed at the SURFsara HPC center in Amsterdam; access was provided via NWO-Rekentijd grant 17569 and 11116 (to T.H. and J.D.C.C.). This work was supported by an ERC-CoG (726072) and NWO VICI (VI.C.182.020) grant awarded to J.D.C.C.

REFERENCES

(1) (a) Padwa, A.; Murphree, S. Epoxides and aziridines - a mini review. *ARKIVOC* **2006**, *2006*, 6−33. (b) Crotti, P.; Pineschi, M. In *Aziridines and Epoxides in Organic Synthesis*; Yudin, A. K., Ed.; Wiley, Hoboken, 2006, pp. 271−313. (c) Smith, J. G. Synthetically Useful Reactions of Epoxides. *Synthesis* **1984**, *1984*, 629−656.

(2) (a) Schneider, C. Synthesis of 1,2-Difunctionalized Fine Chemicals through Catalytic, Enantioselective Ring-Opening Reactions of Epoxides. *Synthesis* **2006**, *2006*, 3919−3944. (b) Vilotijevic, I.; Jamison, T. F. Epoxide-Opening Cascades in the Synthesis of Polycyclic Polyether Natural Products. *Angew. Chem., Int. Ed.* **2009**, *48*, 5250−5281. (c) Rolfe, A.; Samarakoon, T. B.; Hanson, P. R. Formal [4+3] Epoxide Cascade Reaction via a Complementary Ambiphilic Pairing Strategy. *Org. Lett.* **2010**, *12*, 1216−1219. (d) Loertscher, B. M.; Zhang, Y.; Castle, S. L. Exploration of an epoxidation−ring-opening strategy for the synthesis of lyconadin A and discovery of an unexpected Payne rearrangement. *Beilstein J. Org. Chem.* **2013**, *9*, 1179−1184.

(3) (a) Calvani, F.; Crotti, P.; Gardelli, C.; Pineschi, M. Regiochemical control of the ring opening of 1,2-epoxides by means of chelating processes. 8. Synthesis and ring opening reactions of cis- and trans- oxides derived from 3-benzyloxycyclohexene and 2-benzyloxy-5,6-dihydro-2*H*-pyran. *Tetrahedron* **1994**, *50*, 12999−13022. (b) Chini, M.; Crotti, P.; Flippin, L. A.; Gardelli, C.; Macchia, F. Regiochemical Control of the Ring Opening of 1,2-Epoxides by Means of Chelating Processes. 4. Synthesis and Reactions of the *Cis*- and *Trans*-Oxides Derived from 3-[(Benzyloxy)Methyl]-Cyclohexene. *J. Org. Chem* **1992**, *57*, 1713−1718. (c) Chini, M.; Crotti, P.; Flippin, L. A.; Macchia, F.; Pineschi, M. Regiochemical Control of the Ring-Opening of 1,2-Epoxides by Means of Chelating Processes. 2. Synthesis and Reactions of the *Cis*- and *Trans*-Oxides of 4-[(Benzyloxy)Methyl]Cyclohexene, 3-Cyclohexenemethanol and Methyl 3-Cyclohexenecarboxylate. *J. Org. Chem* **1992**, *57*, 1405−1412. (d) Chini, M.; Crotti, P.; Flippin, L. A.; Macchia, F. Regiochemical Control of the Ring-Opening of 1,2-Epoxides by Means of Chelating Processes. 3. Aminolysis and Azidolysis of the *Cis*- and *Trans*-Oxides Derived from 4-(Benzyloxy)Cyclohexene. *J. Org. Chem* **1991**, *56*, 7043−7048.

(4) Fürst, V. A.; Plattner, P. A. Über Steroide Und Sexualhormone. 160. Mitteilung. 2α, 3α- Und 2β, 3β-Oxido-Chlolestane; Konfiguration Der 2-Oxy-Cholestane. *Helv. Chim. Acta* **1949**, *32*, 275−283.

(5) (a) Deora, N.; Carlier, P. R. A Computational Study of Regioselectivity in Aluminum Hydride Ring-Opening of *Cis*- and *Trans*- 4-*t*-Butyl and 3-Methylcyclohexene Oxides. *Org. Biomol. Chem.* **2019**, *17*, 8628−8635. (b) Kas'yan, L. I.; Kas'yan, A. O.; Golodaeva, E. A. Methods and Mechanisms of Epoxy Compounds Reduction. *Russ. J. Org. Chem.* **2008**, *44*, 153−183.

(6) Fleming, I., Frontier Orbitals and Organic Chemical Reactions, Wiley, New York, 1976. New edition: I. *Fleming, Molecular Orbitals and Organic Chemical Reactions;* Wiley, New Jersey, 2009.

(7) (a) Hamlin, T. A.; Fernández, I.; Bickelhaupt, F. M. How Dihalogens Catalyze Michael Addition Reactions. *Angew. Chem., Int. Ed.* **2019**, *58*, 8922−8926. (b) Vermeeren, P.; Hamlin, T. A.; Fernández, I.; Bickelhaupt, F. M. How Lewis acids Catalyze Diels−Alder Reactions. *Angew. Chem., Int. Ed.* **2020**, *59*, 6201−6206. (c) Vermeeren, P.; Brinkhuis, F.; Hamlin, T. A.; Bickelhaupt, F. M. How Alkali Cations Catalyze Aromatic Diels-Alder Reactions. *Chem. − Asian J.* **2020**, *15*, 1167−1174. (d) Vermeeren, P.; Hamlin, T. A.; Fernández, I.; Bickelhaupt, F. M. Origin of Rate Enhancement and Asynchronicity in Iminium Catalyzed Diels-Alder Reactions. *Chem. Sci.* **2020**, *11*, 8105−8112. (e) Vermeeren, P.; Hamlin, T. A.; Bickelhaupt, F. M.; Fernández, I. Bifunctional Hydrogen Bond Donor-Catalyzed Diels-Alder reactions: Origin of Stereoselectivity and Rate Enhancement. *Chem. − Eur. J.* **2021**, *27*, DOI: DOI: 10.1002/chem.202004496.

(8) (a) Vermeeren, P.; van der Lubbe, S. C. C.; Fonseca Guerra, C.; Bickelhaupt, F. M.; Hamlin, T. A. Understanding Chemical Reactivity Using the Activation Strain Model. *Nat. Protoc.* **2020**, *15*, 649−667. (b) Bickelhaupt, F. M.; Houk, K. N. Analyzing Reaction Rates with the Distortion/Interaction-Activation Strain Model. *Angew. Chem., Int. Ed.* **2017**, *56*, 10070−10086.

(9) (a) van Meer, R.; Gritsenko, O. V.; Baerends, E. J. Physical Meaning of Virtual Kohn-Sham Orbitals and Orbital Energies: An Ideal Basis for the Description of Molecular Excitations. *J. Chem. Theory Comput.* **2014**, *10*, 4432−4441. (b) Bickelhaupt, F. M.; Baerends, E. J. Kohn-Sham Density Functional Theory: Predicting and Understanding Chemistry. In *Reviews in Computational Chemistry*; Lipkowitz, K. B.; Boyd, D. B., Eds.; Wiley-VCH: New York, 2000, Vol. *15*, pp. 1−86.

(10) (a) Hansen, T.; Vermeeren, P.; Haim, A.; van Dorp, M. J. H.; Codée, J. D. C.; Bickelhaupt, F. M.; Hamlin, T. A. Regioselectivity of

Epoxide Ring-Openings via S_N2 Reactions Under Basic and Acidic Conditions. *Eur. J. Org. Chem.* **2020**, 3822−3828. (b) Vermeeren, P.; Hansen, T.; Jansen, P.; Swart, M.; Hamlin, T. A.; Bickelhaupt, F. M. A Unified Framework for Understanding Nucleophilicity and Protophilicity in the S_N2/E2 Competition. *Chem. − Eur. J.* **2020**, *26*, 15538−15548. (c) Vermeeren, P.; Hansen, T.; Grasser, M.; Silva, D. R.; Hamlin, T. A.; Bickelhaupt, F. M. S_N2 versus E2 Competition of F^- and PH_2^- Revisited. *J. Org. Chem.* **2020**, *85*, 14087−14093. (d) Van Bochove, M. A.; Roos, G.; Fonseca Guerra, F.; Hamlin, T. A.; Bickelhaupt, F. M. How Mg^{2+} Ions Lower the S_N2@P Barrier in Enzymatic Triphosphate Hydrolysis. *Chem. Commun.* **2018**, *54*, 3448−3451.

(11) Hansen, T.; Lebedel, L.; Remmerswaal, W. A.; van der Vorm, S.; Wander, D. P.; Somers, M.; Overkleeft, H. S.; Filippov, D. V.; Désiré, J.; Mignot, A.; Bleriot, Y.; van der Marel, G. A.; Thibaudeau, S.; Codée, J. D. C. Defining the S_N1 side of glycosylation reactions: stereoselectivity of glycopyranosyl cations. *ACS Cent. Sci.* **2019**, *5*, 781−788.

(12) Boughlala, Z.; Fonseca Guerra, C.; Bickelhaupt, F. M. Alkali Metal Cation Affinities of Anionic Main Group-Element Hydrides Across the Periodic Table. *Chem. − Asian J.* **2017**, *12*, 2604−2611.

(13) Albright, T. A.; Burdett, J. K.; Whangbo, M. H. *Orbital Interactions in Chemistry*; 2nd ed., Wiley: New York, 2013.

(14) Frisch, M. J.; Trucks, G. W.; Schlegel, H. B.; Scuseria, G. E.; Robb, M. A.; Cheeseman, J. R.; Scalmani, G.; Barone, V.; Mennucci, B.; Petersson, G. A.; Nakatsuji, H.; Caricato, M.; Li, X.; Hratchian, H. P.; Izmaylov, A. F.; Bloino, J.; Zheng, G.; Sonnenberg, J. L.; Hada, M.; Ehara, M. *et al. Gaussian 09 Rev. D.01*, Wallingford CT, 2009.

(15) (a) Becke, A. D. A new mixing of Hartree−Fock and local density-functional theories. *J. Chem. Phys.* **1993**, *98*, 1372−1377. (b) Lee, C.; Yang, W.; Parr, R. G. Development of the Colle-Salvetti correlation-energy formula into a functional of the electron density. *Phys. Rev. B* **1988**, *37*, 785−789. (c) Vosko, S. H.; Wilk, L.; Nusair, M. Accurate spin-dependent electron liquid correlation energies for local spin density calculations: a critical analysis. *Can. J. Phys.* **1980**, *58*, 1200−1211. (d) Grimme, S.; Antony, J.; Ehrlich, S.; Krieg, H. A consistent and accurate *ab initio* parametrization of density functional dispersion correction (DFT-D) for the 94 elements H-Pu. *J. Chem. Phys.* **2010**, *132*, 154104. (e) Grimme, S.; Ehrlich, S.; Goerigk, L. Effect of the damping function in dispersion corrected density functional theory. *J. Comput. Chem.* **2011**, *32*, 1456−1465.

(16) Ditchfield, R.; Hehre, W. J.; Pople, J. A. Self-Consistent Molecular-Orbital Methods. IX. An Extended Gaussian-type basis for molecular-orbital studies of organic molecules. *J. Chem. Phys.* **1971**, *54*, 724−728.

(17) Zhao, Y.; Truhlar, D. G. The M06 suite of density functionals for main group thermochemistry, thermochemical kinetics, noncovalent interactions, excited states, and transition elements: two new functionals and systematic testing of four M06-class functionals and 12 other functionals. *Theor. Chem. Acc.* **2008**, *120*, 215−241.

(18) Weigend, F.; Ahlrichs, R. Balanced basis sets of split valence, triple zeta valence and quadruple zeta valence quality for H to Rn: Design and assessment of accuracy. *Phys. Chem. Chem. Phys.* **2005**, *7*, 3297−3305.

(19) Simón, L.; Goodman, J. M. How reliable are DFT transition structures? Comparison of GGA, hybrid-meta-GGA and meta-GGA functionals. *Org. Biomol. Chem.* **2011**, *9*, 689−700.

(20) Bootsma, A. N.; Wheeler, S. E. Popular Integration Grids Can Result in Large Errors in DFT-Computed Free Energies. *ChemRxiv. Preprint.* **2019**, DOI: 10.26434/chemrxiv.8864204.v4.

(21) Ribeiro, R. F.; Marenich, A. V.; Cramer, C. J.; Truhlar, D. G. Use of solution-phase vibrational frequencies in continuum models for the free energy of solvation. *J. Phys. Chem. B.* **2011**, *115*, 14556−14562.

(22) (a) te Velde, G.; Bickelhaupt, F. M.; Baerends, E. J.; Fonseca Guerra, C.; van Gisbergen, S. J. A.; Snijders, J. G.; Ziegler, T. Chemistry with ADF. *J. Comput. Chem.* **2001**, *22*, 931−967. (b) Fonseca Guerra, C.; Snijders, J. G.; te Velde, G.; Baerends, E. J. Towards an Order-N DFT Method. *Theor. Chem. Acc.* **1998**, *99*, 391−403. (c) *ADF2018.104, SCM Theoretical Chemistry*, Vrije Universiteit: Amsterdam (The Netherlands). www.scm.com.

(23) Sun, X.; Soini, T. M.; Poater, J.; Hamlin, T. A.; Bickelhaupt, F. M. PyFrag 2019−Automating the Exploration and Analysis of Reaction Mechanisms. *J. Comput. Chem.* **2019**, *40*, 2227−2233.

(24) van Lenthe, E.; Baerends, E. J. Optimized Slater-type Basis Sets for the Elements 1−118. *J. Comput. Chem.* **2003**, *24*, 1142−1156.

(25) (a) Lenthe, E. V.; Baerends, E. J.; Snijders, J. G. Relativistic Regular Two-component Hamiltonians. *J. Chem. Phys.* **1993**, *99*, 4597−4610. (b) van Lenthe, E.; Baerends, E. J.; Snijders, J. G. Relativistic Total Energy Using Regular Approximations. *J. Chem. Phys.* **1994**, *101*, 9783−9792.

(26) (a) Franchini, M.; Philipsen, P. H. T.; van Lenthe, E.; Visscher, L. Accurate Coulomb Potentials for Periodic and Molecular Systems Through Density Fitting. *J. Chem. Theory Comput.* **2014**, *10*, 1994−2004. (b) Franchini, M.; Philipsen, P. H. T.; Visscher, L. The Becke Fuzzy Cells Integration Scheme in the Amsterdam Density Functional Program Suite. *J. Comput. Chem.* **2013**, *34*, 1819−1827.

(27) Legault, C. Y., *CYLview, 1.0b*; Université de Sherbrooke, Canada, Sherbrooke, QC, 2009, www.cylview.org.

(28) (a) Ess, D. H.; Houk, K. N. Distortion/Interaction Energy Control of 1,3-Dipolar Cycloaddition Reactivity. *J. Am. Chem. Soc.* **2007**, *129*, 10646−10647. (b) Ess, D. H.; Houk, K. N. Theory of 1,3-Dipolar Cycloadditions: Distortion/Interaction and Frontier Molecular orbital Models. *J. Am. Chem. Soc.* **2008**, *130*, 10187−10198.

(29) (a) Atkins, P., De Paula, J., *Physical Chemistry*, Edition 9, Oxford University Press, Oxford, 2010. (b) Jensen, F., *Introduction to Computational Chemistry*, Edition 2, Wiley, West Sussex, 2007.

https://dx.doi.org/10.1021/acs.joc.0c02955
J. Org. Chem. 2021, 86, 3565−3573